Research Article

Health monitoring of bolted joints using modal-based vibrothermography

Xintian Chi[1] · Dario Di Maio[2,3] · Nicholas A. J. Lieven[1]

Received: 21 January 2020 / Accepted: 23 July 2020

Abstract
This article presents a novel modal-based vibrothermographic approach for health monitoring of loosening bolted joints in coupled structures. In this article, the theoretical background supporting this proposed approach is firstly presented. Through finite element analyses on a simple bolted structure with varying joint conditions achieved by adjustment of bolt loads, the relationship between the bolt load and the temperature increase in the vibrating bolted joint during vibrothermographic tests was revealed. Experimental vibrothermographic tests on a more complex structure were completed to verify the observations from the finite element analyses while demonstrating the viability of the vibrothermographic approach in a laboratory environment. It has been shown that this vibrothermographic approach was able to determine the stage of a bolted joint in its progression of failure by tracing the changes in the temperature increase in relevant regions during vibrothermographic tests. Moreover, additional tests have been performed to illustrate that this approach was effective even by using only the residual responses of the structure's vibration that were away from the resonances, which indicates it is more applicable to structures with higher damping as such structures have stronger residual responses during vibration that can be utilized. In the concluding observations of the article, the procedure for practical application of this approach is summarized, and its potential for further development is discussed.

Keywords Structural health monitoring · Infrared thermography · Vibrothermography · Bolted joint · Modal analysis · Finite element analysis

1 Introduction

Due to continuous advances in engineering and manufacturing industries, many engineering structures have been becoming increasingly complex. One of the most common elements in these complex structures is joints which are used to connect individual components. However, joints are able to introduce complicated dynamics to the structures, which have to be understood so that the structures connected by joints can be designed accordingly and operated safely.

Among the common types of joints in engineering structures, bolted joints have been one of the most-studied types of joint due to their varying dynamic properties under different loading and contact conditions. Firstly, it was demonstrated that the uncertainty and nonlinear characteristics in joints, particularly bolted joints, are able to cause a range of complex dynamic problems, adding to the fact that the sources of these characteristics in joints usually vary from case to case [1]. The nonlinear behaviors caused by bolted joints were also studied by Gaul and Lenz, where a finite element (FE) model was created to study the stick–slip mechanism in the contact

✉ Xintian Chi, xintian.chi@bristol.ac.uk | [1]Department of Aerospace Engineering, University of Bristol, Bristol, England, UK. [2]Department of Mechanical Engineering, University of Twente, Enschede, Netherlands. [3]Department of Mechanical Engineering, University of Bristol, Bristol, England, UK.

Published online: 29 July 2020

area, which is one of the main causes of the complicated dynamic behaviors in joints [2]. Schwingshackl et al. [3] and Hartwigsen et al. [4] also managed to utilize FE analyses to model and study the nonlinear behaviors in bolted flange joints and a shear lap joint respectively. In terms of experimental tests, Ma et al. showed the possibility of using laser vibrometer to identify the dynamics of bolted joints [5]. Di Maio et al. also achieved successful results in identifying and locating nonlinearities in joints using strain analysis [6] and scanning laser vibrometer [7]. In addition to the variability of dynamics in joints, Chi et al. demonstrated that there is also mutual influence between the dynamic and the thermal parameters in vibrating bolted joints under different loading and contact conditions [8].

Besides their complicated dynamics originated from a range of sources, joints, specifically bolted joints, also tend to develop problems in operating conditions which correspondingly alter the dynamic properties and can affect the performance and threaten the integrity of the structure.

There have been research activities and associated articles suggesting potential techniques for detecting defective joints and evaluating joint integrity in engineering structures. Firstly, the utilization of ultrasonic approaches, which are the de-facto standard techniques for damage detection in engineering industries, has been studied [9, 10]. Using samples from responsive space satellites as the specimen, Doyle et al. applied acoustoelastic and electromechanical impedance methods for detecting defective bolted joints [11]. In addition, Argatov and Sevostianov demonstrated that electrical conductivity measurements could be utilized for detecting the loosening failure of conductive bolted joints [12]. Shin et al. [13] and Zagrai et al. [14] have shown the possibility of using piezoelectric active sensors for health monitoring of joints. Giurgiutiu et al. [15] and Pavelko et al. [16] have also achieved positive results from health monitoring of spot-welded lap-shear joints and bolted joints respectively using the electromechanical impedance technique. Moreover, Kim and Wang suggested an enhancement to the electromechanical impedance approach by using piezoelectric circuitry [17].

However, the utilization of infrared thermography (IRT), which is one of the most commonly deployed nondestructive testing and evaluation techniques, has been rarely studied for detection of joint problem and evaluation of joint integrity in engineering structures. IRT as a damage detection and structural health monitoring approach has several distinct advantages, such as being able to perform rapid continuous non-contact scans of large areas with short measurement times [18]. The results from IRT inspections are usually presented in the form of whole-field two-dimensional images or videos, which are easy to understand hence able to lower the difficulty of the subsequent data analyses. These advantages make IRT practically viable for detection of damage and monitoring of health in large-scale engineering structures due to its high effectiveness and efficiency.

During the failing process, dynamic properties of bolted joints are changed due to altered contact conditions. As studied by the authors, the dynamic and thermal properties in vibrating bolted joints are interrelated, both of which are affected by different loading and contact conditions [8]. For this reason, in this article, a novel approach using modal-based vibrothermography, which is a special application of IRT, is presented and applied to study the thermal behaviors in vibrating bolted joints at different integrity conditions, through which the changes in dynamic properties in bolted joints at different integrity conditions can be revealed using temperature data. With the relationship between the temperature and the integrity condition of bolted joints revealed, the stage of a bolted joint in its failing process can be determined. Specifically, loosening failure of bolted joints is selected as the type of problem to be studied as it is arguably the most common type of problem of bolted joints. In this research, the loosening process was simulated by the application of different bolt loads.

This modal-based vibrothermographic approach has been studied by the authors and verified on detecting sub-surface damage, specifically delamination, in aerospace-grade composite materials [19]. In this research, this proposed approach is extended to be applied to coupled structures connected by bolted joints, which are relevant to a wider range of engineering products. Both numerical simulations using the FE analysis and experimental tests were performed in this research. In the FE analyses, a simple coupled structure consisting of two components connected by a bolt was created and studied, while a more complex metal frame structure consisting of four bolted joints, each having six different interfaces, was used as the specimen for the experimental tests. Through the FE analyses, the relationship between the bolt load simulating integrity condition of the bolted joint and the temperature increase during vibrothermographic tests was revealed, which has then been verified in the experimental vibrothermographic tests.

2 Theoretical background

Vibrothermography is a special application of IRT that utilizes friction in relevant regions, such as the interfaces and damaged areas, of an inspected structure as the heat source [20]. In vibrothermography, the inspected structure is excited by mechanical forces or acoustic/ultrasonic waves at a single frequency—or multiple frequencies—so that the relevant regions produce friction

due to relative motion between surfaces during the induced vibration, which leads to local heat generation that can be detected by an infrared (IR) camera. Because of the friction-based heat generation mechanism, vibrothermography is more suitable than the conventional heat-flow-based IRT approaches for this research. Specifically, through vibrothermographic tests, changes of dynamic characteristics in joints, which are caused by altered joint conditions, can be revealed through analyses of thermal data, as changes in the former are able to affect the frictional heat generation considerably.

In vibrothermographic tests, in order to ensure adequate frictional heat generation that can be detected by an IR camera, the inspected regions need to have sufficient strain energy during vibration, otherwise detectable heat will not be generated in these regions which means the vibrothermographic approach is compromised [19, 21].

For a vibrating structure, high strain energy is achieved around resonances, at which the response of the structure is maximized. For this reason, the calculation of strain energy distribution in the structure can be achieved by a modal analysis. Specifically, the modal analysis is able to measure experimentally and/or numerically calculate the natural frequencies (resonant frequencies) of a structure, as well as the mode shape and the associated strain energy distribution at each resonance. In operating conditions, the deflection shape of a structure is a combination of all excited mode shapes so that calculating the strain energy distribution in each mode of vibration is able to predict the actual strain energy distribution in the structure [22].

For active vibrothermographic testing specifically where external excitation is applied to the inspected structure to induce vibration, with the necessary knowledge of the distribution of strain energy at each resonance, parameters of the excitation force can be selected to ensure high strain energy concentration in the inspected regions during the structure's vibration.

During vibrothermographic testing, the inspected structure vibrates due to the applied excitation. The heat will be generated due to friction created by relative motion between surfaces in relevant regions, such as the damaged areas, defects and interfaces, inside the inspected structure during the induced vibration, which can be captured by an IR camera.

In this research, the relative motion between the contact surfaces in the joints is rather complicated and can be described as a stick–slip process [23–26]. However, despite the complex nature of the stick–slip motion, as the objective of this research is to study the heat generation in joints through friction, the stick portion which does not provide frictional heat generation was not concerned.

For the sake of completeness, even when there is zero relative motion between two surfaces, heat will still be generated through other mechanisms such as the thermoelastic effect and plasticity-induced heat generation [20, 27]. However, the heat generated through these mechanisms is usually considerably lower than the heat generated from friction, especially when the relative motion between the contact surfaces is significant compared to the overall elastic and plastic deformation in the joint region of the structure, which is the case in this research. For this reason, it was safe to assume that the temperature increases in the joints being inspected in the experimental tests of this research were due to frictional heat generation. Separately, as frictional heat generation was defined as the only heat generation mechanism in the FE analyses of this research, all heat generation and temperature increases recorded in the FE analyses were completely caused by friction.

When relative motion is present, the frictional heat generation rate between two contact surfaces can be calculated from:

$$P = F_f \dot{\gamma} \tag{1}$$

where F_f is the frictional force which equals to the normal force F_n multiplied by the kinetic friction coefficient μ_k and $\dot{\gamma}$ is the slip rate which is the speed of the relative motion between the contact surfaces [20, 28].

For frictional heat generation in the vibrating bolted joints being studied in this research, both of the parameters were affected by the contact condition in the bolted joints. Practically, as a bolted joint starts to loosen, the contact load between the surfaces will decrease, which correspondingly result in a reduction in normal force while an increase in slip rate. For this reason, it may be predicted that, during vibrothermographic tests, if all other parameters such as amplitude and frequency of vibration remain approximately unchanged, a maximum frictional heat generation rate exists, which corresponds to a specific contact load level in the joint. In this case, as a sound bolted joint becomes loose, the frictional heat generation is expected to increase first, and then decrease as it is approaching failure so that a bell-curve-shaped relationship can be observed.

This prediction can be demonstrated using a simplified mathematical model. Firstly, we can isolate the joint region by modelling the effects from other regions of the structure as a damper and a spring. For a pair of contact surfaces in the joint region, if we take the lower element as the reference surface, the equation of motion of the upper part of the interface can be written as:

$$m\ddot{\gamma} + c\dot{\gamma} + k\gamma = F \tag{2}$$

where F in this case is the kinetic friction force F_f, which can be calculated from:

$$F_f = \mu_k F_n \tag{3}$$

F_n is the total normal force which, for the specific case in this research, consists of the bolt load and other normal forces such as the mass of the structure supported by the joint.

In order to estimate the relationship between the contact load and frictional heat generation, we can simplify the problem by assuming that the external force from the rest of the structure onto the joint, which has been simulated as a damper and a spring in Eq. 2, is constant and only exists in shear direction, denoted as F_e, while assuming the kinetic friction coefficient μ_k is constant as well. In this case, the frictional heat generation rate at any moment t is:

$$P = F_f \dot{\gamma} = \mu_k F_n \dot{\gamma} = \mu_k F_n \frac{F_e - \mu_k F_n}{m} t \tag{4}$$

The maximum can be easily calculated, which is achieved when:

$$F_{n\_max} = \frac{F_e}{2\mu_k} \tag{5}$$

From Eq. 5, it can be observed that the normal force corresponding to the maximum frictional heat generation rate is directly proportional to the external shear force exerted onto the joint in this situation.

If the external force is not constant, the force applied to the isolated joint also becomes a variable. However, the general relationship between normal force and frictional heat generation rate still exists. This implies that, for a joint region, the normal force at which the maximum frictional heat generation rate is reached is still positively correlated with the external shear force applied to the joint. The progression of failure in a bolted joint that decreases the normal force F_n may either increase or decrease the frictional heat generation rate depending on the relationship between the current F_n and F_{n_max}.

Realistically, due to the fact that the kinetic friction coefficient is usually velocity-dependent and that the external force is usually time-dependent while existing in multiple directions, deriving a unifying mathematical model describing the exact relationship between the frictional heat generation rate and the normal force—or contact condition—in joints is almost impossible, especially considering that the dynamic properties of joints may even change under different temperatures due to thermal expansion and deformation [29].

However, it is possible to rely on FE analyses to observe the changes of frictional heat generation in bolted joints at varying contact load levels representing different bolted joint conditions, instead of pursuing a unifying quantitative relationship through mathematical derivations.

3 Finite element analysis

In order to study the thermal behaviors in joints through numerical vibrothermographic tests in an FE environment, a simple model of a coupled structure was created in SIMULIA Abaqus, where the reason for using a simple model was to ensure that unexpected factors could be reduced to as minimum as possible. Specifically, the model consisted of a cuboid as the base and a cube as the top, which were connected by a bolt. During the analyses, the load in the bolt could be adjusted to achieve different contact conditions in the joint. The dimensions of the cuboid were 0.3 m × 0.05 m × 0.02 m. The side length of the cube was 0.05 m. The created FE model is shown in Fig. 1.

A solid homogeneous section using the properties of mild steel was created to define this FE model. Specifically, the density was set to 7850 kg/m^3. The Young's modulus was 211 GPa and the Poisson's ratio was 0.303. The thermal conductivity was 45 W/(mK). The specific heat capacity was 510 J/(kg K). The element type was C3D4T, which is a four-node thermally coupled tetrahedron [30]. The element size determined after mesh convergence was 0.004 m with a 10% minimum size control.

For the definition of the interfaces, the static-kinetic friction model was used as the tangential behavior, where the static friction coefficient was set to 0.7 and the kinetic friction coefficient was set to 0.6 [31]. As for the normal behavior, the "hard" contact definition was used to prevent penetration between the contact surfaces [32]. Penetration between surfaces is one of the most common sources of inaccuracies and errors in FE analyses if defined inappropriately. Heat generation and thermal conductance were also included to enable frictional heat generation and heat transfer between the components. Specifically, Abaqus calculated frictional heat generation using the relationship

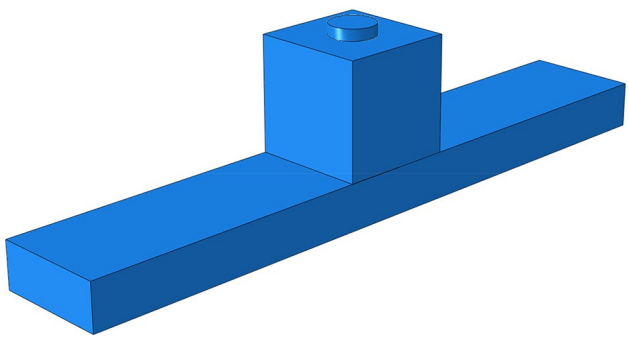

Fig. 1 The FE model created in SIMULIA Abaqus

described in Eq. 1 [28] and it was defined that all energy dissipated through friction was converted to heat.

The FE vibrothermographic tests were to be performed using the explicit dynamic coupled temperature-displacement analysis in Abaqus to achieve high accuracies by including the interactions between the dynamic and thermal effects. As explained previously, in order to perform a reliable vibrothermographic test, the dynamic behaviors of the structure must be studied to obtain the relevant stress and strain distributions, which could be achieved by completing a modal analysis. Specifically, the results from the modal analysis served the role of selecting frequency and location of the excitation force used in the active vibrothermographic tests so that detectable heat could be generated in relevant regions during the induced vibration.

In this research, an FE modal analysis was performed in SIMULIA Abaqus, where the Lanczos method was used to calculate the eigenvalues and eigenvectors that corresponded to the natural frequencies and mode shapes of the structure [33]. The mode shape and natural frequency of the structure in the first and second mode of vibration are shown in Fig. 2, and the corresponding strain energy distributions were calculated and superimposed on the mode shapes, as displayed in Fig. 3. In the modal analysis and the subsequent vibrothermographic simulations, a free-free boundary condition was applied which ensured free movement of the structure without extra constraints so that the effects from unexpected external factors could be minimized.

From the results in Fig. 2, it can be observed that in the first mode, the structure only moved in Z-direction, while in the second mode, the motion was generally—but not completely—in the X–Y plane. This difference was able to affect the frictional heat generation in the joint during vibrothermographic tests significantly, so the two modes of vibration were studied separately, which will be demonstrated later in this section. In addition, the strain energy distributions shown in Fig. 3 have revealed that in both modes the contact region possessed high strain energy concentration so that both modes were suitable for vibrothermographic tests because of their capabilities of generating considerable heat in the interface through friction during vibration.

After completion of the modal analysis, the FE vibrothermographic simulations could be performed. As explained previously, the simulation of different joint conditions was achieved by adjustment of bolt load. In order to apply bolt load prior to the execution of the FE vibrothermographic simulations, static analyses needed

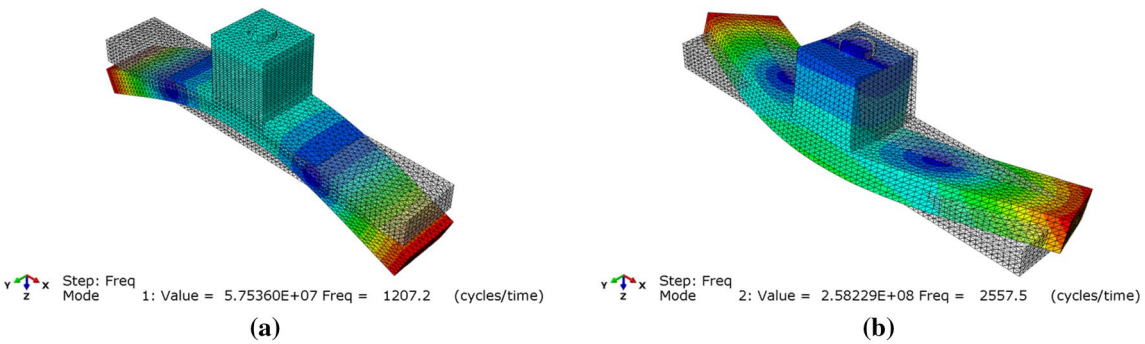

Fig. 2 Mode shape and natural frequency of the structure in the **a** first and **b** second mode of vibration

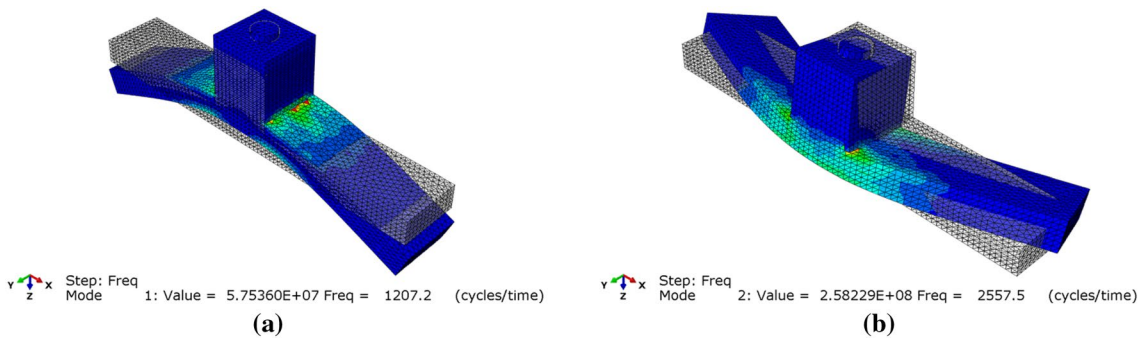

Fig. 3 Strain energy distribution in the structure in the **a** first and **b** second mode of vibration

to be completed. In the static analyses, the bolt load was applied at the middle surface of the bolt as a uniformly distributed force parallel to the direction of the bolt's axis. For this structure, it was decided to apply 40 levels of bolt load, which spanned from 250 to 10,000 N with increments of 250 N.

Following the static analyses, it was additionally verified that the natural frequencies of the structure were not significantly altered by the different bolt load so that consistency could be assured across the different simulations. Next, results from the static analyses were imported into the corresponding explicit dynamic coupled temperature-displacement analyses as the initial states using the Abaqus "Predefined Fields" function [34] so that the changes caused by the application of the bolt load could be taken into consideration during the vibrothermographic simulations. Before the start of the simulations, an initial temperature of 20 °C was defined for the whole model.

In each explicit dynamic coupled temperature-displacement analysis that simulated a vibrothermographic test, a harmonic external force was applied to excite the structure. As the two modes of vibration were studied separately, the frequency of the excitation force was set to match the corresponding natural frequency, which was 1207.2 Hz for the first mode and 2557.5 Hz for the second mode. The location and direction of the excitation force for each mode are shown in Fig. 4 so that the target mode could be excited effectively. Three different amplitudes were used for the excitation force, which were 500 N, 1000 N and 1500 N respectively. With 40 different levels of bolt load, this gave 120 sets of data for each mode of vibration so that the reliability and repeatability of the results could be assured. Due to the extreme computation time and power required for an explicit dynamic coupled temperature-displacement analysis, each analysis only simulated 0.05 s. However, this was sufficient to cover 60 cycles and 127 cycles of vibration for the first and second mode respectively.

After the completion of the FE analyses, the reliability of the results was verified for each mode of vibration by observing the temperature profiles of multiple elements in the contact interface across multiple analyses. Between the two modes of vibration, the second mode is presented first, as the motion in the joint is predominantly in-plane which more closely resembled the circumstance described previously in the theoretical background section.

3.1 The second mode of vibration, FE analysis

During the data validation, it was observed that the elements in the contact interface displayed similar temperature profiles over the simulation period. Among the inspected elements, results from two elements, namely element 25,936 and element 5473, are presented here as examples. Both elements were located on the top surface of the cuboid base inside the contact region. The exact locations of the two elements are shown in Fig. 5.

Temperature increases, which were solely caused by frictional heat generation due to the definition of the FE model, at element 25,936 and element 5473 at the end of the analyses were calculated and plotted in Fig. 6. In each plot, as all parameters apart from bolt load were kept constant, the results can be compared on the same basis.

From the results in Fig. 6, multiple notable behaviors can be observed.

Firstly, as predicted previously, for unchanged excitation parameters (amplitude and frequency), when the bolt load increases, the normal force will increase while the slip rate will decrease. This will result in the existence of a maximum frictional heat generation rate so that the relationship between the friction heat generation rate, which was represented here by the temperature

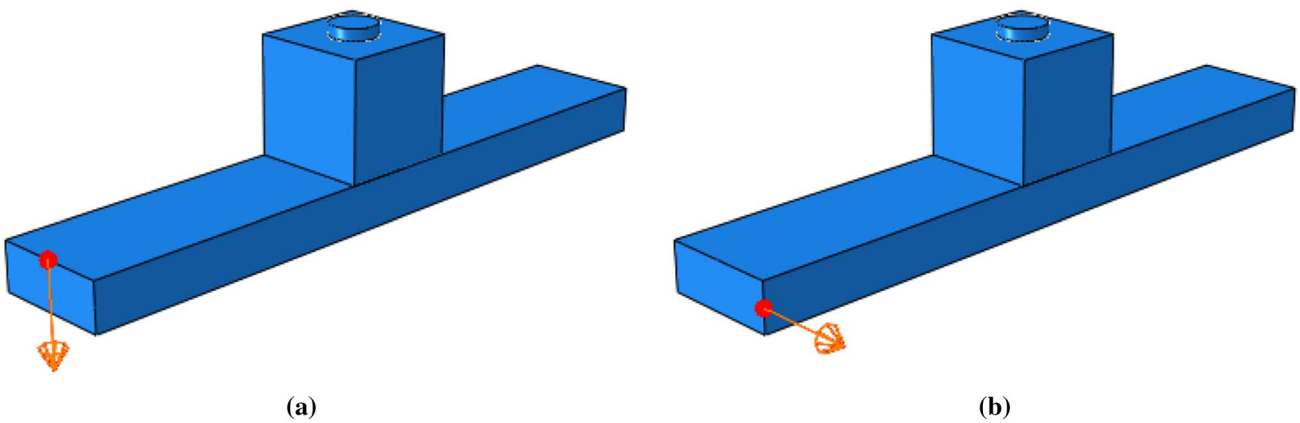

Fig. 4 Location and direction of excitation force for the **a** first and **b** second mode of vibration

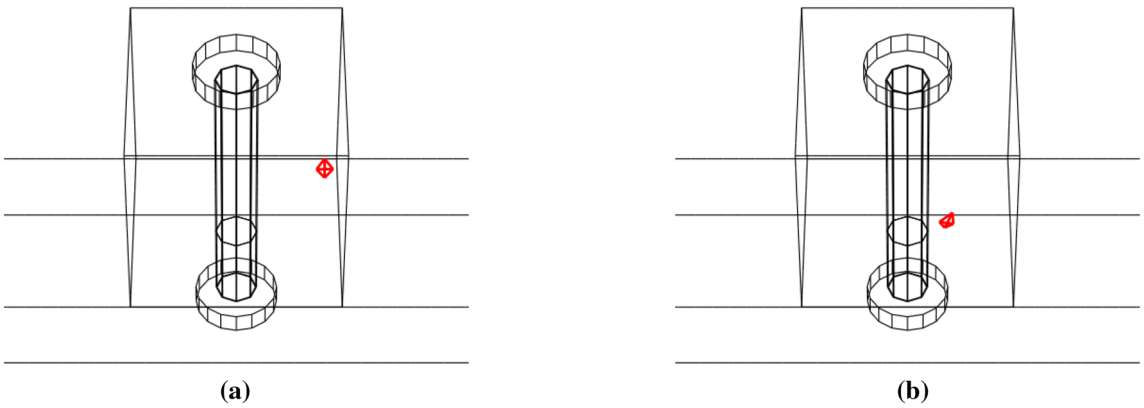

Fig. 5 Location of **a** element 25,936 and **b** element 5473

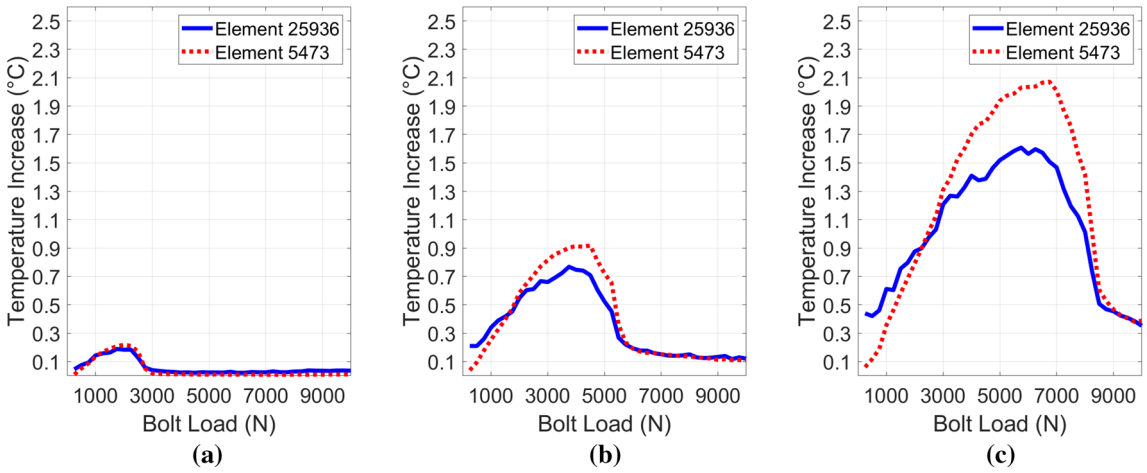

Fig. 6 Temperature increase (°C) over 0.05 s with **a** 500 N, **b** 1000 N and **c** 1500 N excitation amplitude, the second mode of vibration

increase over a fixed amount of time, and bolt load can be approximately described as a bell curve.

This behavior is clearly demonstrated in Fig. 6. It was also observed that the bolt load corresponding to the maximum frictional heat generation rate was positively correlated with the external force, which conformed with the prediction made in the theoretical background section. Additionally, the amplitude of the external force was also positively correlated with the width of the peak of frictional heat generation.

For unchanged bolt load, as the excitation amplitude increased, the frictional heat generation rate ascended as well. The relationship was not linear firstly due to the stick–slip motion since as the excitation amplitude increased, the portion of the stick motion was reduced, which enhanced the frictional heat generation even further. Another main reason for the nonlinearity was the altered contact condition, which will be explained shortly.

Moreover, the normal force and the slip rate varied across locations in the contact interface, so the frictional heat generation rate was always different at different positions. The exact distributions of normal force, slip rate and frictional heat generation rate always depend on the shape of the structure during vibration. Although the absolute value of the frictional heat generation rate varied at different locations, the shapes of the curves, including the bolt load corresponding to the maximum frictional heat generation rate and the width of the peak, tended to be similar at different locations in the same contact interface when the other parameters remained unchanged, as shown in Fig. 6 a–c.

Among the two parameters determining the frictional heat generation, it is obvious that the frictional force is positively correlated with bolt load. However, it was mentioned previously that as bolt load increases, the slip rate between the contact surfaces should always decrease, which in fact was not entirely a reflection of the true

behavior. To demonstrate this effect, the accumulated slip distances over 0.05 s at element 25,936 and element 5473 were summarized to represent the average slip rates and displayed in Fig. 7.

The primary observation is that the relationship between slip distance and bolt load was not monotonic. Although seemingly counter-intuitive, this behavior could be explained. At low bolt load, surfaces often lost contact during vibration. The slip rate in the affected regions could be considered negligible in these situations due to the loss of contact. As the bolt load increased, the loss of contact became less frequent. In this case, the average slip rate increased with the bolt load. After a point where the loss of contact became more consistent through the cycles, the average slip rate started to decrease as the bolt load continued to increase due to ascending friction caused by increasing normal force. It was observed that the relationship between average slip rate and bolt load can also be approximated as a bell curve, as shown in Fig. 7. The loss of contact was verified by extracting the average areas of contact between the two surfaces during vibration, which are shown in Fig. 8.

In can be observed that when the bolt load was low, the average area of contact was considerably smaller compared to that at high bolt load, which demonstrated the frequent loss of contact between the surfaces at low bolt load levels during vibration.

For unchanged bolt load, the different excitation forces also altered the area of contact. A larger excitation force aggravated the loss of contact, which made the maximum average slip rate appear at a higher bolt load and created a wider peak, as shown in Fig. 7. This

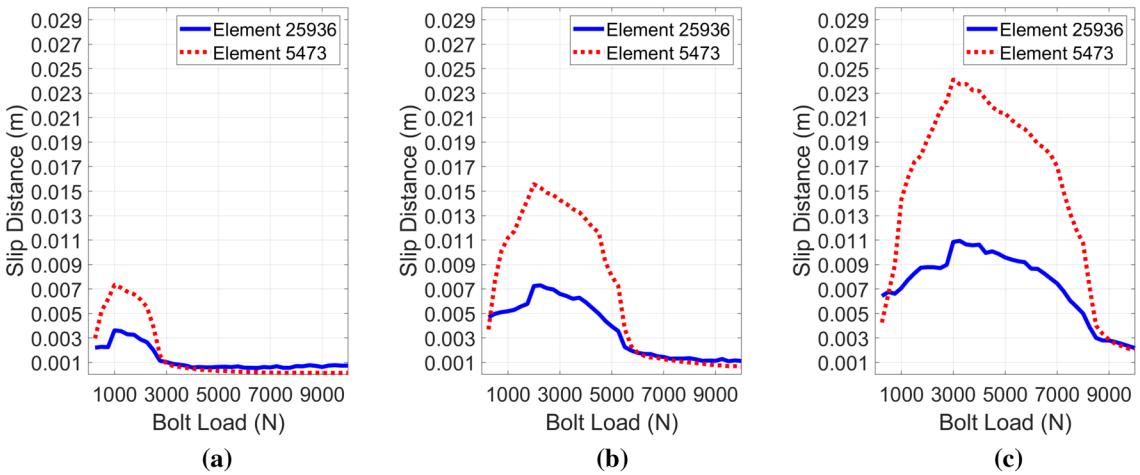

Fig. 7 Slip Distance (m) over 0.05 s with **a** 500 N, **b** 1000 N and **c** 1500 N excitation amplitude, the second mode of vibration

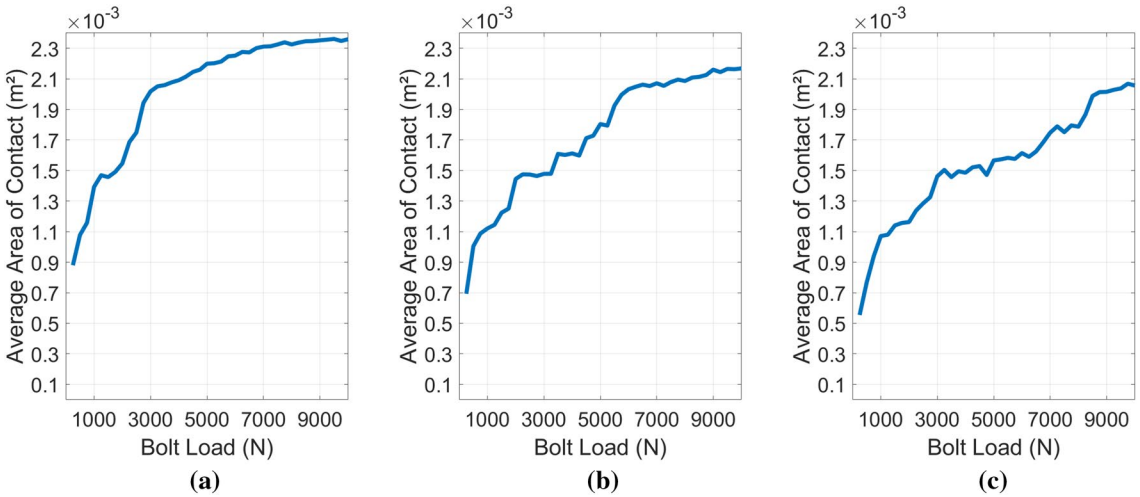

Fig. 8 The average area of contact (m^2) over 0.05 s with **a** 500 N, **b** 1000 N and **c** 1500 N excitation amplitude, the second mode of vibration

observation leads directly to the nonlinear association between the frictional heat generation rate and the excitation amplitude.

To summarize, although there was a moderate loss of contact between the surfaces during vibration so the relationship between the average slip rate and the bolt load was not monotonic, a bell-curve-shaped relationship could still be observed between frictional heat generation and bolt load due to the loss of contact being relatively insignificant. The practical interpretation of this observation is that, as a bolted joint goes through its loosening process, the frictional heat generation rate inside the joint will firstly increase, then decrease as the failure approaches. However, the same trend was not observed in the first mode of vibration, where the loss of contact became more significant.

3.2 The first mode of vibration, FE analysis

For the first mode of vibration, results from two new elements are presented here as examples due to changes in temperature distribution because of different deformation shape of the structure during vibration. The locations of the two new elements, namely element 13,366 and element 8792, are shown in Fig. 9. Similar to the case in the second mode of vibration, both elements were located on the top surface of the cuboid base inside the contact region.

The temperature increases at element 13,366 and element 8792 at the end of the analyses were collected and plotted as shown in Fig. 10.

As observed in Fig. 10, the relationship between the temperature increase and the bolt load became monotonic. Although this behavior violated the anticipation made in the previous section, it could be explained through the loss of contact. The loss of contact was again

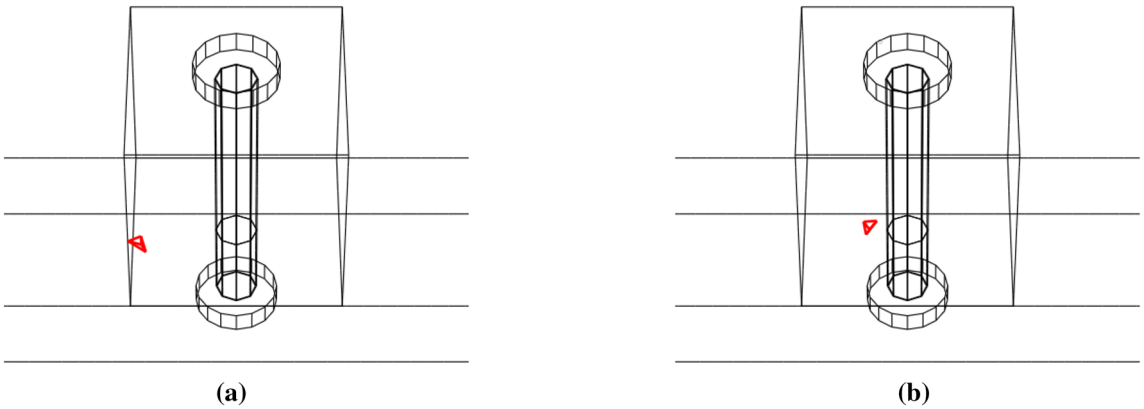

Fig. 9 Location of **a** element 13,366 and **b** element 8792

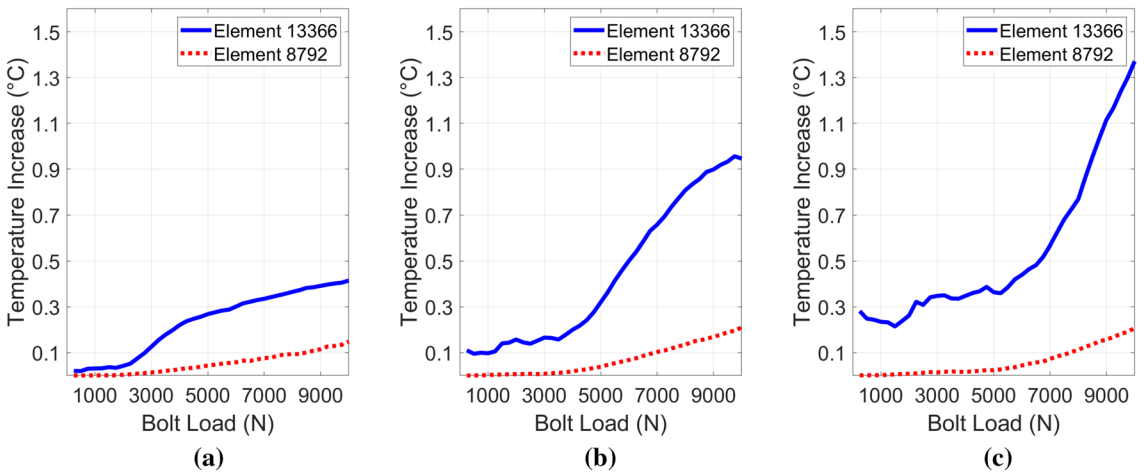

Fig. 10 Temperature increase (°C) over 0.05 s with **a** 500 N, **b** 1000 N and **c** 1500 N excitation amplitude, the first mode of vibration

demonstrated by extracting the average area of contact between the two surfaces during vibration, which is shown in Fig. 11.

By comparing the values in Figs. 8 and 11, it can be observed that the loss of contact was more pronounced in the first mode of vibration because the motion of the structure was in Z-direction in this mode. For this reason, the lack of heat generation during the loss-of-contact phase became significant so that the originally anticipated bell-curve-shaped relationship between frictional heat generation and bolt load was altered entirely, which became monotonic.

Specifically, the influence of the loss of contact was revealed using the accumulated slip distance data, which are plotted in Fig. 12.

It can be observed from Fig. 12 that the influence of the loss of contact became so dominant that the slip distance and the bolt load became approximately positively correlated. In this case, the average slip rate increased correspondingly with bolt load until a significant bolt load was reached so that the loss of contact became relatively less frequent.

Due to the frequent loss of contact, both the normal force and the average slip rate tended to be positively correlated with the bolt load until the bolt load was relatively high, which resulted in a monotonic relationship between temperature increase through friction and bolt load, as shown in Fig. 10.

However, despite the observations from the first mode of vibration, it must be noted that the opening force

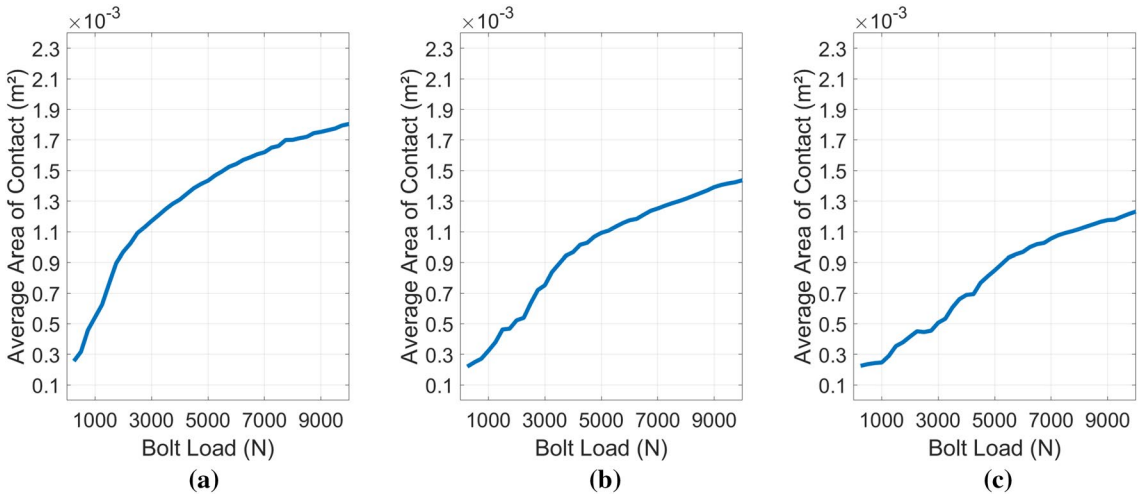

Fig. 11 The average area of contact (m^2) over 0.05 s with **a** 500 N, **b** 1000 N and **c** 1500 N excitation amplitude, the first mode of vibration

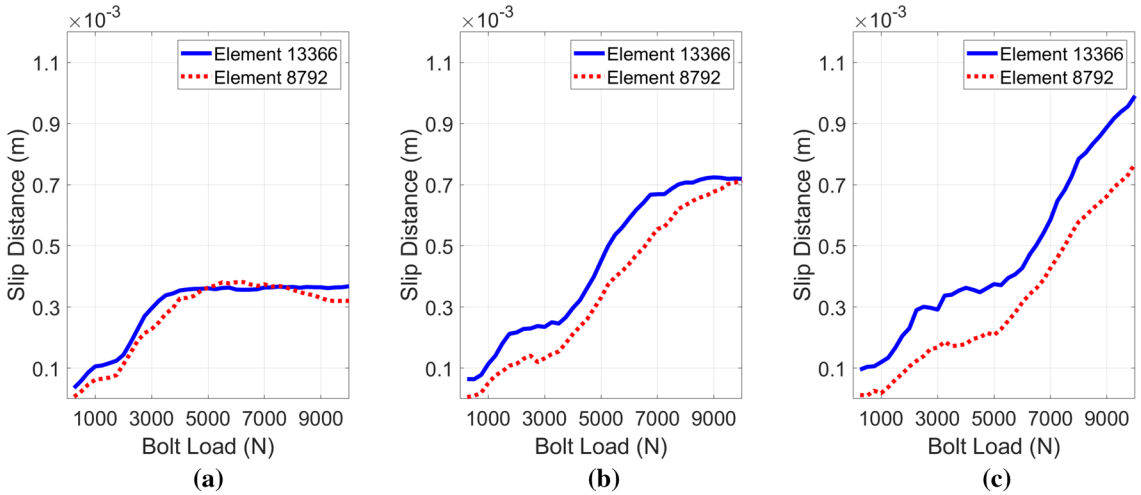

Fig. 12 Slip Distance (m) over 0.05 s at element 13,366 with **a** 500 N, **b** 1000 N and **c** 1500 N excitation amplitude, the first mode of vibration

normal to the contact surfaces must be significant, such as the case in this research, for the effects from loss of contact to be so dominant that the originally anticipated bell-curve-shaped relationship is altered entirely. If the loss of contact is not as significant, a bell-curve-shaped relationship as observed in the second mode of vibration should be expected.

4 Experimental testing

In order to further verify the observations found in the FE analyses as well as showing the viability of this modal-based vibrothermographic approach in a practical environment, experimental vibrothermographic tests have been performed.

4.1 Rig setup for experimental testing

The structure being studied experimentally was a metal frame structure consisting of four bolted joints located at the four corners. The structure was made of mild steel and had a mass of 10.3 kg. The structure was suspended throughout the tests to minimize the influence of unexpected external factors that may affect the heat generation in the structure during the vibrothermographic tests. The suspended structure and the drawing of the joint are shown in Fig. 13. The reason behind using a more complex structure in the experimental tests was to verify that the conclusions acquired from the simple structure in FE analyses would still apply in a more complicated scenario, which could be helpful for the generality and practicality of this modal-based vibrothermographic approach.

4.2 Experimental modal testing

Firstly, as described previously, a modal analysis should be performed before the vibrothermographic tests. Specifically, the objective of the initial modal analysis is to measure experimentally and/or numerically calculate the modal parameters, including natural frequency, mode shape and strain energy distribution of the structure in each mode of vibration so that an appropriate mode can be selected for the vibrothermographic test. With an appropriately selected mode of vibration where the region of interest has high local strain energy, the effectiveness of the excitation force can be maximized in terms of the amount of frictional heat generation in the interested region caused by the excitation.

As demonstrated in the previous section, apart from the experimental modal analysis (EMA), a modal analysis also consists of the portion of the FE analysis. Specifically, although the modal parameters of a structure can be obtained through an EMA, the FE analysis is able to provide localized specificity with considerably higher resolution due to the limitations on the number of sensors that can normally be placed on a structure in an experimental test. For this reason, performing FE modal analyses in addition to the EMA is usually beneficial for acquiring more detailed information of the studied structure.

When the FE analysis is considered, a preliminary FE modal analysis is usually performed before the experimental testing to estimate the modal parameters of the structure so that a more reliable selection of the location and frequency range for the excitation force can be deployed in the EMA. After the completion of the EMA, the preliminary FE model can be subject to model updating so that it can provide results which are more accurate representations of the properties of the physical structure. However, model updating is not always mandatory if the preliminary model is able to provide sufficient information in the regions of interest in the structure.

After realizing the significance of the modal analysis before the actual vibrothermographic tests, the initial modal analyses should be implemented. In this research, because only one joint in the metal frame structure was to be inspected during the vibrothermographic tests, the loads on the other three bolts were lowered to zero to

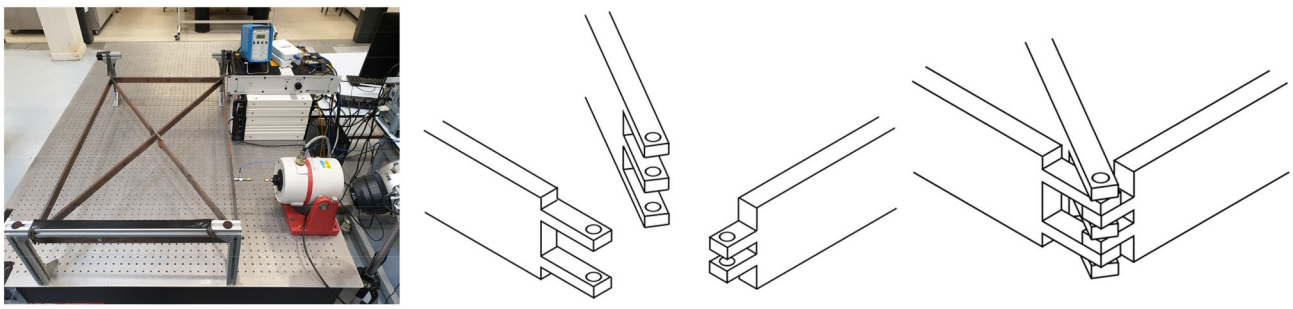

Fig. 13 The **a** suspended metal frame structure and **b** drawing of the joint [35]

reduce damping in the structure so that the frictional heat generation could be concentrated on the inspected joint. The bolt load in the inspected joint was set to 6 Nm for both the physical structure and the preliminary FE model, which was approximately the maximum load that could be applied by hand on the bolt in the physical structure. However, for the sake of completeness, the total normal force in the other three joints was still not equal to zero due to the mass of the structure that was supported by the joints.

Following the completion of the preliminary FE modal analysis, based on which the frequency range of interest was selected to be 10 Hz to 100 Hz, experimental tests were performed on the metal frame structure. The first 10 natural frequencies measured from the EMA are summarized in Table 1 and the mode shapes are shown in Fig. 14.

4.3 FE modal analysis on the updated model

Following the EMA, the preliminary FE model was updated based on the experimental results, after which the outputs from the FE modal analysis became almost identical to the results from EMA. The high-fidelity mode shapes of the first 10 modes of vibration from the FE analysis are shown in Fig. 15. By comparing the mode shapes shown in Figs. 14 and 15, nine out of the 10 modes of vibration could be correlated. The fifth mode of vibration was an out-of-plane mode, so it was unable to be excited using an in-plane excitation force, which explained its absence from the EMA results. Apart from the fifth mode, all other modes were correlated and the comparisons between their natural frequencies are summarized in Table 2.

The updated FE model was able to achieve a satisfactory correlation with the experimental results. Among the nine correlated mode pairs, eight mode pairs had a natural frequency difference smaller than 3%, with five lower than 1%. These observations demonstrated that the updated FE model was able to provide reliable representations of the actual structure.

The strain energy distributions for the first 10 modes of vibration were then extracted from the FE results to assist the target mode selection. To reiterate, the mode of vibration used for the vibrothermographic tests must be carefully selected so that the region of interest has high local strain energy, thus ensuring the frictional heat generation can be maximized. To reflect this behavior, the strain energy distribution in the inspected joint in each mode of vibration is shown in Fig. 16, where an equal rainbow-based color scale was applied to all plots to allow more convenient comparisons of results.

Among the 10 modes of vibration displayed in Fig. 16, multiple modes had relatively high strain energy in the inspected joint, which were mode 5, mode 7, mode 9 and mode 10. To optimize the selection, alongside the strain energy, the other factor that needed to be considered was how easily each mode could be excited. Specifically, for electrodynamic shakers, exciting a location with greater mode shape in the direction of the excitation force is able to excite the corresponding mode of vibration more energetically. Among the four candidates listed above, the fifth mode of vibration was an out-of-plane mode that could not be used, as explained previously. The seventh and ninth modes of vibration could not be conveniently

Table 1 Natural frequencies of the first 10 modes of vibration, EMA

Mode	1	2	3	4	5	6	7	8	9	10
Freq. (Hz)	11.05	17.63	21.86	27.32	54.15	57.42	60.13	62.44	77.56	97.48

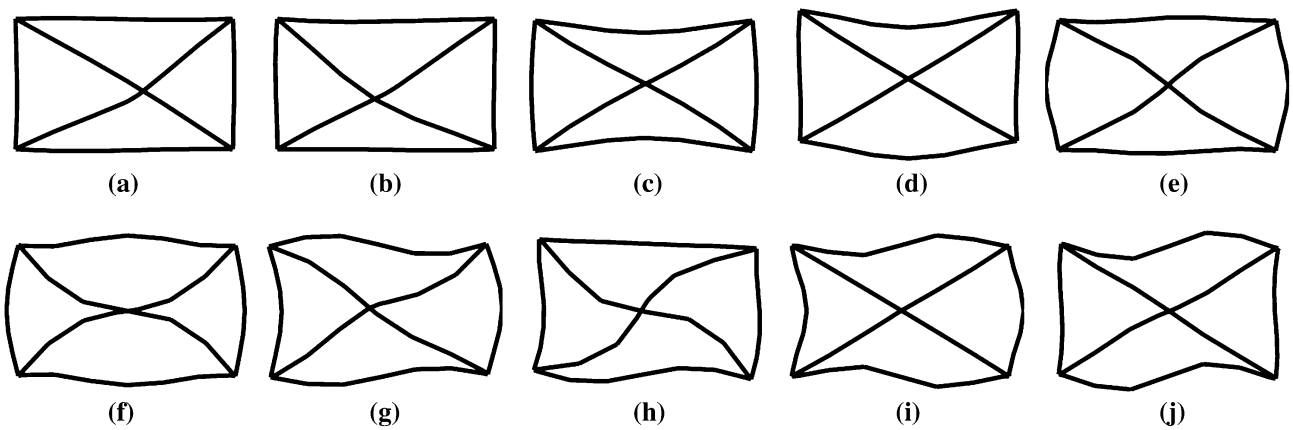

Fig. 14 Mode shapes of the **a**–**j** first-10th modes of vibration, EMA [35]

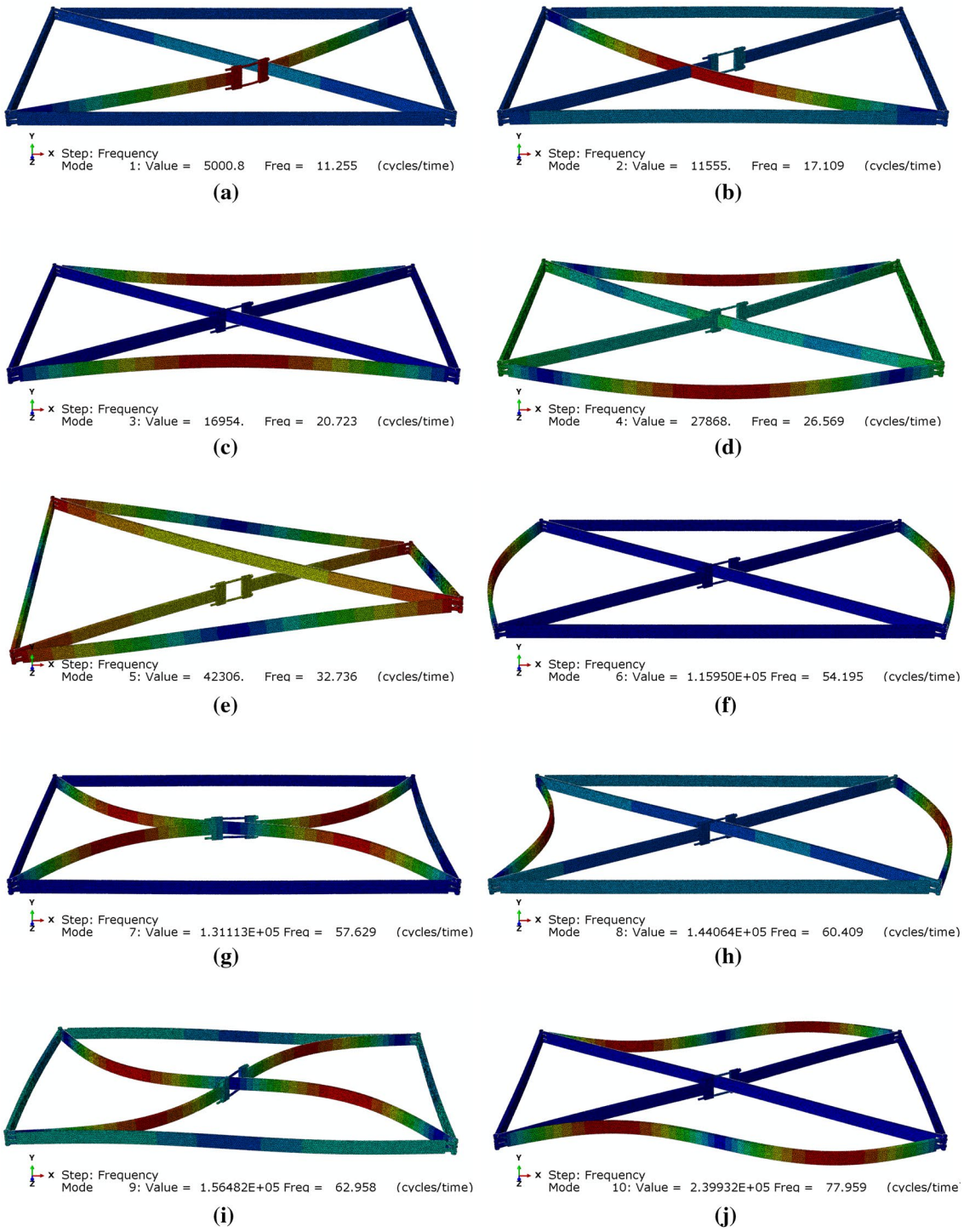

Fig. 15 Mode shapes of the **a**–**j** first-10th modes of vibration, FE modal analysis

Table 2 Natural frequencies of the first 10 modes of vibration, EMA vs FE modal analysis

Mode	1	2	3	4	5	6	7	8	9	10
Freq. EMA (Hz)	11.05	17.63	21.86	27.32	N/A	54.15	57.42	60.13	62.44	77.56
Freq. FE (Hz)	11.26	17.11	20.72	26.57	32.74	54.20	57.63	60.41	62.96	77.96
Diff. (%)	1.90	-2.95	-5.22	-2.75	N/A	0.09	0.37	0.47	0.83	0.52

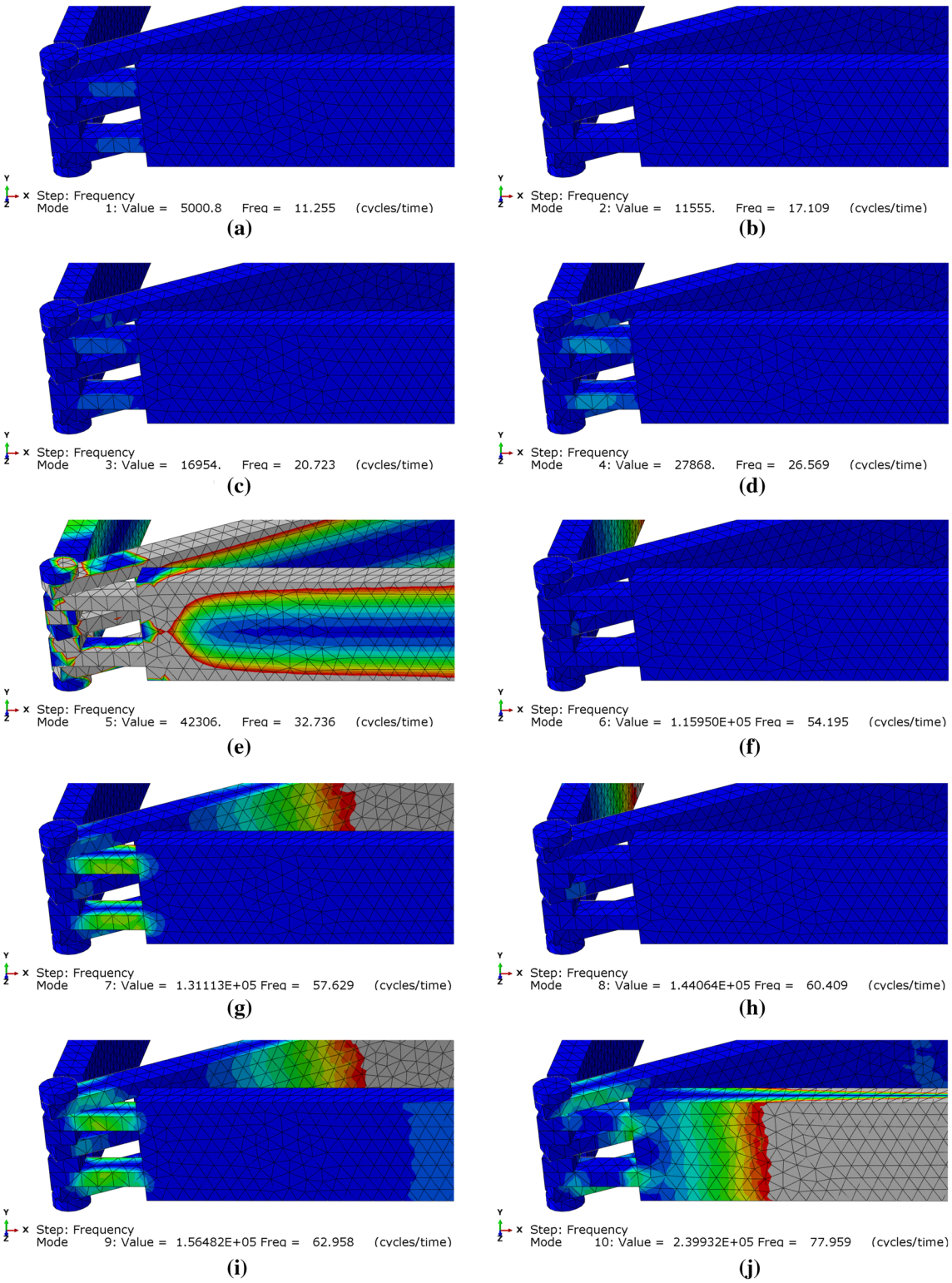

Fig. 16 Strain energy distributions in the joint, the **a**–**j** first-10th modes of vibration, FE modal analysis

excited as the locations of maximum mode shape were not easily accessible, which left the 10^{th} mode of vibration the only suitable choice. As shown in Fig. 15, the location with maximum mode shape in the 10th mode of vibration was easily accessible, so this mode of vibration could be pertinently excited in the vibrothermographic tests.

4.4 Experimental vibrothermographic testing

As described previously, the 10th mode of vibration was selected for the experimental vibrothermographic tests. An electrodynamic shaker was attached at the location with the maximum mode shape in this mode of vibration to achieve highest excitation efficiency, as shown in Fig. 13a.

As the objective was to demonstrate that there could be detectable heat generation due to friction in the inspected joint and to verify the relationship between the frictional heat generation and the bolt load level representing different joint conditions, six magnitudes of bolt load were selected. The six levels of bolt load are listed in Table 3, which were precisely applied using a digital torque wrench. As explained in the previous sections, because only one joint was to be inspected in the vibrothermographic tests, changes were only applied to the bolt in the inspected joint, whilst loads on the other three bolts were kept at zero.

Additional EMA was performed at each bolt load level to ensure that the bolt load was successfully applied and that the changes in natural frequency of the 10th mode of vibration would not cause a significant difference in the dynamic behavior of the structure. During the tests, the parameters of the signal generator and the power amplifier remained unchanged. The natural frequency and damping ratio of the 10th mode of vibration at each bolt load level were measured and summarized in Table 3.

As displayed in Table 3, as the bolt load decreased, the natural frequency of the 10th mode of vibration descended correspondingly due to the changes in stiffness, which indicated that the bolt load was successfully applied. The relationship between the damping ratio and the bolt load, however, was not monotonic, which will be explained later in this section.

During the vibrothermographic tests, the frequency of the excitation force was set to match the natural frequency of the 10th mode of vibration and the amplitude of the excitation force was kept approximately constant from the case in the EMA by using the same parameters for the signal generator and power amplifier, which remained unchanged across all the vibrothermographic tests. For data acquisition, a Nippon Avionics TH9100MR IR camera was used to measure the temperature data. The camera has a resolution of 320×240 and a thermal sensitivity of 0.02 °C, which makes it capable of capturing the subtle changes in temperature in the inspected structure during the vibrothermographic tests. In all six tests, data were recorded at 10-s intervals. The timeline of the vibrothermographic tests is summarized in Table 4, which was replicated in all six tests. Because of the identical parameters used during the six tests and the same times at which data are captured, the data acquired during different tests could be compared on the same basis.

Data recording had been started before the electrodynamic shaker was turned on in order to capture the initial temperature data, which were then subtracted from the other frames to reveal the net temperature increase. After the shaker was turned off, the measurement continued for another five minutes to capture the heat dissipation process to ensure that no unexpected circumstances had happened during the tests. The first example snapshots from the six tests mentioned in Table 4, which were taken at five minutes after the shaker was turned on, are shown in Fig. 17. The second example snapshots taken at 10 min after the shaker was turned on are shown in Fig. 18. In all snapshots, the initial temperature data captured before the shaker was turned on were subtracted so that temperature values in the images indicated net increases. The snapshots were sorted in descending order according to the bolt load (6.0 Nm, 4.5 Nm, 3.0 Nm, 1.5 Nm, 0.5 Nm and 0 Nm). An equal temperature scale that spanned from 0 to 4 °C was used for all snapshots to enable more convenient comparisons of results across different tests.

Firstly, it was demonstrated that the friction between the contact surfaces in the joint was able to generate clearly detectable hot spots. In fact, for all bolt load levels except the zero-load case, multiple hot spots with maximum temperature increases higher than 0.5 °C became observable within two minutes after the shaker was turned on. The frictional heat generation was also significantly more rapid than the heat dissipation so that highly

Table 4 Timeline of events in the vibrothermographic tests

Time (min:sec)	Event
0:00	Data recording was started
2:00	The electrodynamic shaker was turned on
7:00	The example snapshots displayed in Fig. 17 were taken
12:00	The electrodynamic shaker was turned off The example snapshots displayed in Fig. 18 were taken
17:00	Data recording was stopped

Table 3 Natural frequency and damping ratio of the 10th mode of vibration at different bolt load levels

Bolt load (Nm)	0	0.5	1.5	3.0	4.5	6.0
Frequency (Hz)	75.44	75.97	76.32	76.79	77.15	77.56
Freq. change (%)	−2.73	−2.05	−1.60	−0.99	−0.53	0
Damping ratio (%)	1.22	1.55	2.70	2.10	1.73	1.78

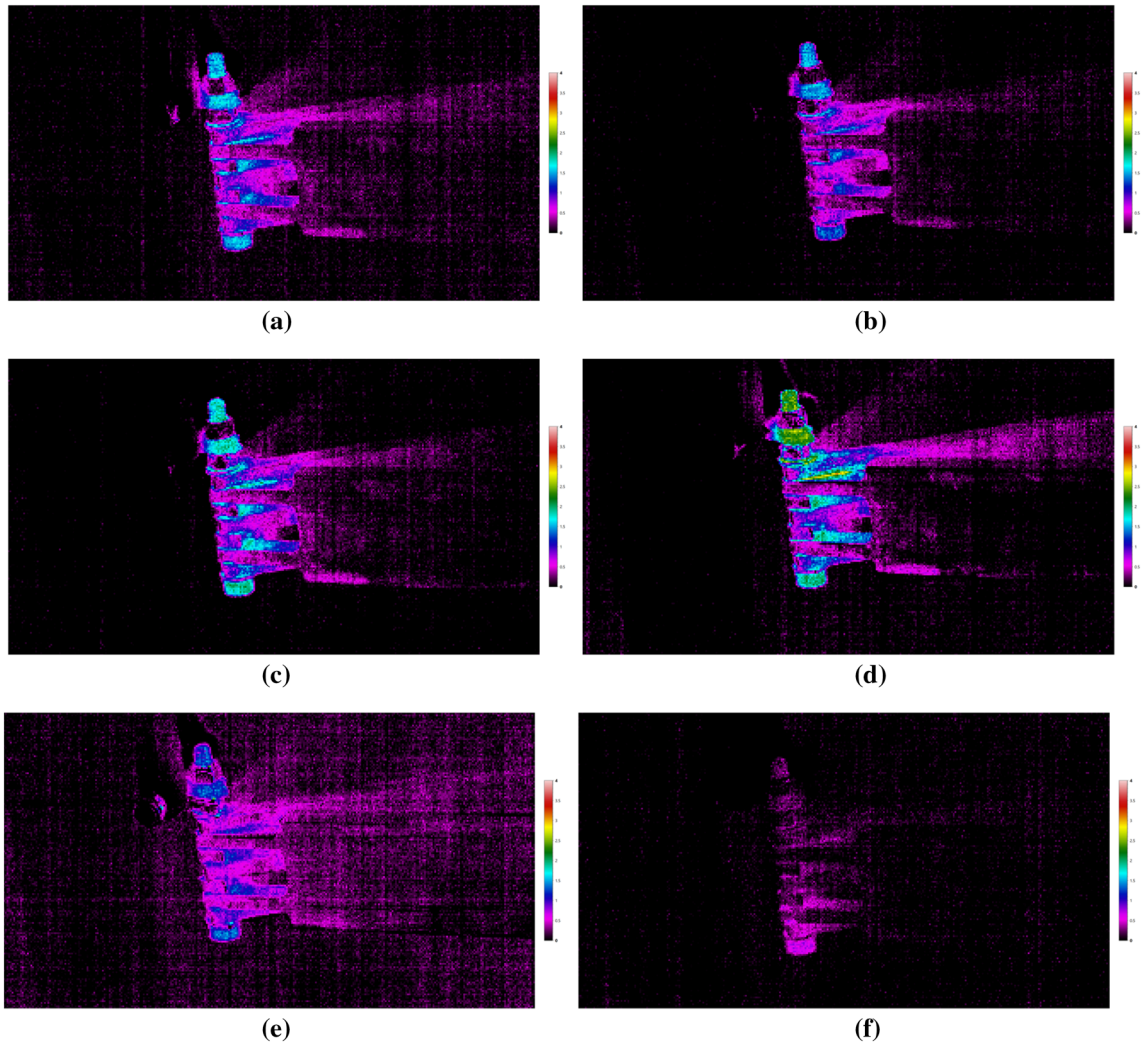

Fig. 17 The first snapshots from the six tests, sorted in descending order by bolt load (**a**–**f** 6.0 Nm, 4.5 Nm, 3.0 Nm, 1.5 Nm, 0.5 Nm and 0 Nm)

localized hot spots were developed. These observations have successfully verified the possibility of using vibrothermography to detect loosening bolted joints in coupled structures with the advantage of short measurement time.

In order to compare the results from the different tests quantitatively, the topmost interface in the inspected joint was selected for value probing. To achieve this, a rectangular measurement box was added surrounding the topmost interface, as shown in Fig. 19, in order to measure the maximum temperature increase in this region. The maximum temperature increases in the topmost interface in the snapshots shown in Figs. 17 and 18, which were captured at five minutes and 10 min after the electrodynamic shaker was turned on respectively, were extracted and plotted as shown in Fig. 20.

By inspecting the snapshots in Figs. 17, 18 and the plot in Fig. 20, it can be observed that, for data captured at the same times across the tests with identical setup and unchanged parameters, as the bolt load decreased, which simulated a continuously degrading integrity condition of the bolted joint, the frictional heat generation rate represented by the temperature reading firstly increased, until a maximum was reached, and then started to decrease rapidly.

Additionally, the trend of temperature increase corroborated with the changes in damping ratio summarized in Table 3, which is plotted in Fig. 21, due to the reason that the majority of the energy dissipation in the structure was through frictional heat generation.

By comparing the experimental results summarized in Fig. 20 and the FE outputs displayed in Fig. 6, it can be observed that the relationship between the frictional heat generation rate and the bolt load followed a similar bell-curve-shaped trend. Specifically, in the mode of vibration

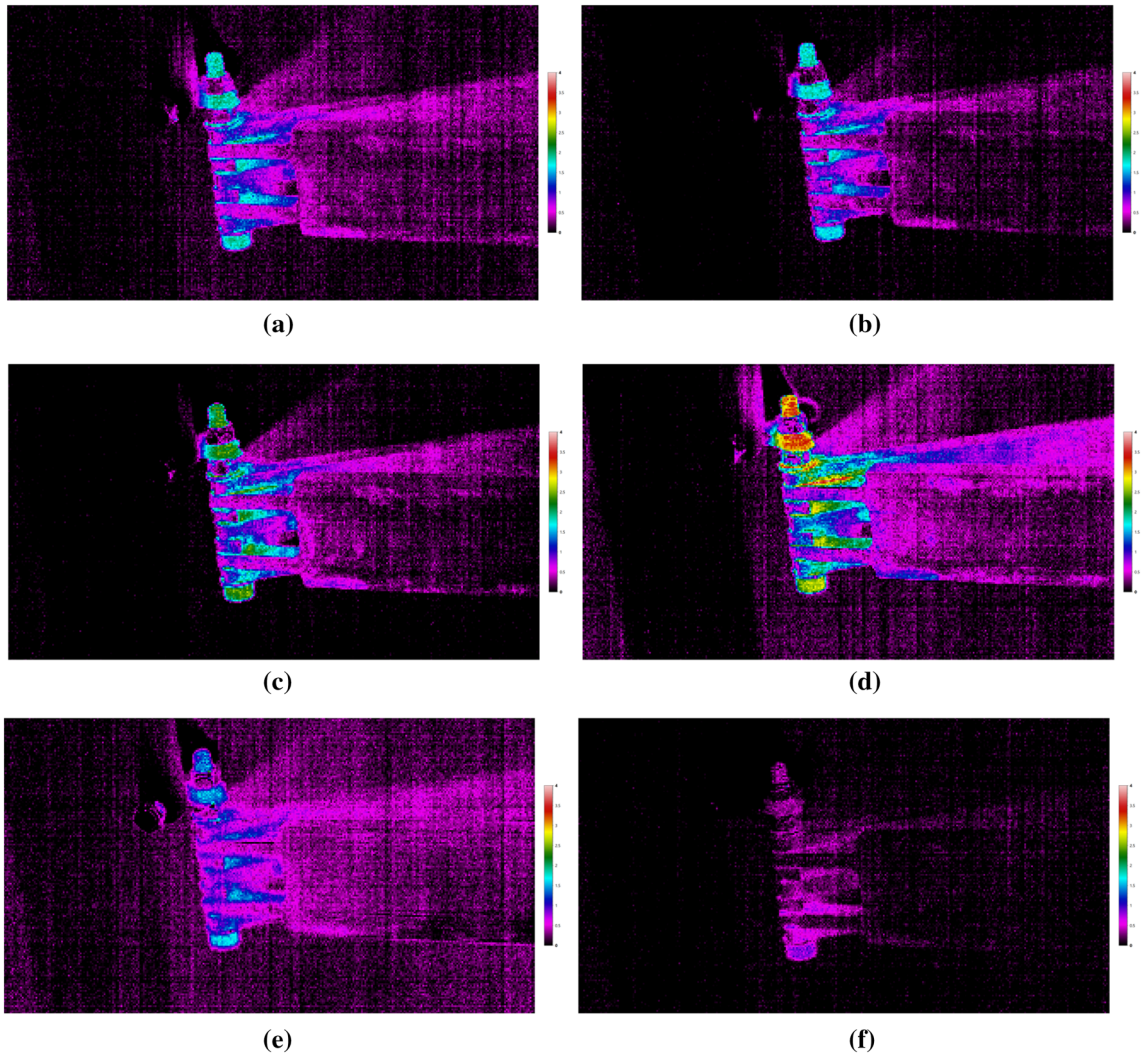

Fig. 18 The second snapshots from the six tests, sorted in descending order by bolt load ((a)-(f) 6.0 Nm, 4.5 Nm, 3.0 Nm, 1.5 Nm, 0.5 Nm and 0 Nm)

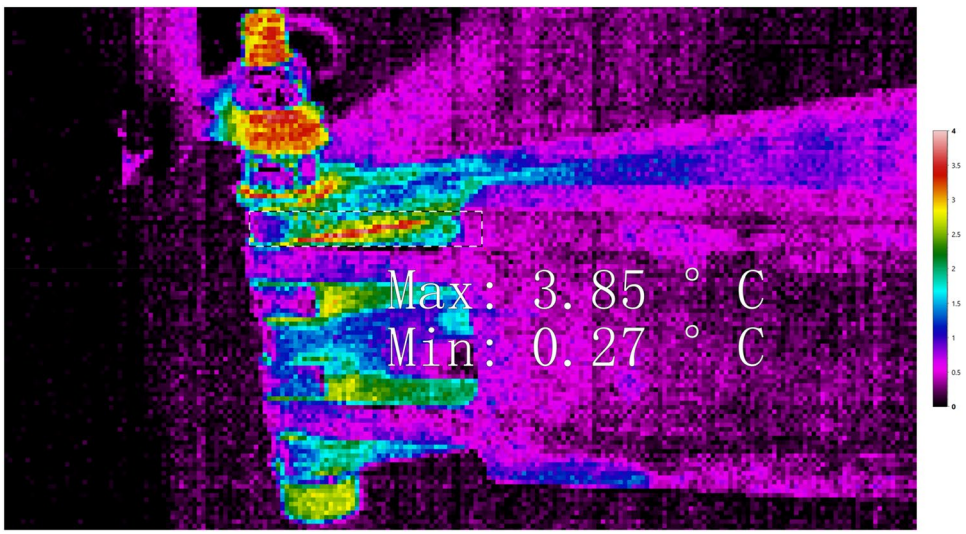

Fig. 19 The box created around the topmost interface to measure the maximum temperature increase

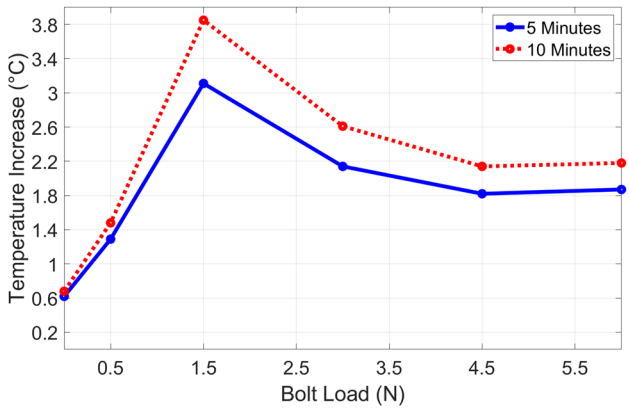

Fig. 20 Maximum temperature increase (°C) in the topmost interface recorded at five and 10 min after the electrodynamic shaker was turned on

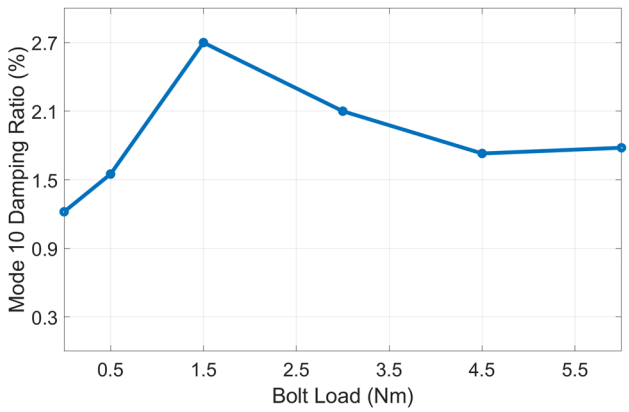

Fig. 21 The damping ratio of the 10th mode of vibration at different bolt load levels

selected for the experimental tests, there was approximately zero out-of-plane motion in the structure, which means the loss of contact between the surfaces was negligible. For this reason, the results from the experimental tests resembled those from the second mode in FE analyses instead of the first mode where the loss of contact was significant.

The experimental results have verified that when the loss of contact between surfaces in the joint was insignificant, the frictional heat generation rate would firstly increase, then decrease as the bolted joint's integrity condition approaches failure, given that other major parameters such as amplitude and frequency of vibration in the inspected structure remained approximately unchanged.

Separately, the similarity between the relationship of the temperature increase and the damping ratio versus the bolt load, as shown in Fig. 20 and Fig. 21 respectively, indicates that it is possible to utilize temperature to estimate damping ratio in certain applications. This is specifically useful for inaccessible structures and regions where contact measurement methods are unable to be applied so that damping data can be difficult to obtain.

Apart from the major observations in terms of the relationship between the frictional heat generation and the bolt load, another characteristic was apparent. As demonstrated in Figs. 17 and 18, although following a similar trend, the exact distribution of frictional heat generation was not identical across the different interfaces. It is possible that this observation was an indication that the interfaces had different contact loads, which could be a result of two potential factors.

Firstly, assuming that the distribution of bolt load was uniform across the interfaces, the lower interfaces tended to have a higher contact load as they supported a greater portion of the structure's own mass.

Secondly, it is likely that the distribution of bolt load was not uniform across the interfaces, which would add more uncertainties to the differences in contact loads between the interfaces.

However, in order to discover the exact reasons behind this interesting phenomenon, additional tests need to be performed, which may be explored in future research.

5 Consideration of residual responses in vibrothermographic tests

Thus far in this research, it has been demonstrated the viability of detecting the condition change and revealing the relationship between the frictional heat generation and the progression of degradation of bolted joints in two representative structures through FE and experimental vibrothermographic tests, in which the parameters such as the frequency and the location of the excitation force were carefully selected.

In some practical applications, however, passive vibrothermography, in which the structures are subject to operationally induced vibration, so no extra external force is required, is likely to have higher relevance to users than the active vibrothermography that requires additional excitation force.

The advantage of passive vibrothermography is the removal of requirements on additional external excitation forces. However, the vibration of structure in the passive vibrothermography is less well-controlled so the frequencies at which the structures vibrate rarely uniquely match the natural frequency of a single mode of vibration with usable strain energy in the region of interest, especially for rotating machinery that usually operates at a constant rate of rotation.

But this does not indicate that passive vibrothermographic tests are unlikely to succeed. For a damped structure, an excitation force with a dominant single frequency is able to excite multiple modes of vibration by exciting the residual responses of modes of vibration whose natural frequencies are not identical to the excitation frequency. Although not at the peak response, the partially excited modes are still able to provide a certain level of strain energy in the inspected region, which can be sufficient for vibrothermographic tests. This phenomenon can be surprisingly useful considering that the complex structures used in industries tend to have higher damping than the simpler structures used in laboratories due to their functional complexity. In this situation, the residual responses are also greater, which lowers the requirements on the frequency and the amplitude of vibration correspondingly.

This speculation has been verified experimentally on the metal frame structure used in this research, which had moderate damping that varied with several factors, such as the bolt load and the mode of vibration, as demonstrated in Table 3.

In this experimental test, the structure was excited at the natural frequency of the second mode of vibration with the other parameters such as the location of the excitation force and the boundary condition of the structure remaining the same as in the previous tests. This was not expected to cause a high level of response of the second mode as the mode shape of the second mode of vibration was considerably low at the point of excitation, according to the mode shape in Fig. 14b and Fig. 15b. Even if the second mode was excited, there was almost zero strain energy in the inspected joint in this mode, as indicated by the strain energy distribution in Fig. 16b. The load on the bolt in the inspected joint was set to 0.5 Nm to lower the frictional heat generation rate even further in order to add extra challenges artificially. Due to these reasons, the second mode alone was not anticipated to provide detectable frictional heat generation.

In this test, the procedure described in Table 4 was still strictly followed. Two example snapshots were taken at the same times as in the previous six tests, i.e. at five minutes and 10 min respectively after the shaker was turned on. The two snapshots are shown in Fig. 22. The initial temperature data were captured and subtracted from the snapshots. The temperature scale remained the same as in the previous results, which spanned from 0 to 4 °C.

As observed in Fig. 22, in contrast to the original expectation, the contact surfaces were able to generate clearly detectable heat. This response could only be attributed to the third mode of vibration being excited. The third mode had a natural frequency of 18.2 Hz when the bolt load was 0.5 Nm on the bolt in the inspected joint and 0 Nm on the other three bolts, which was close to the natural frequency of the second mode of vibration that was 15 Hz in the same condition. For this reason, it is believed that it was the third mode of vibration being excited that provided the frictional heat generation in the joint, which was detected by the IR camera, instead of the second mode of vibration which was unable to generate sufficient heat for the reasons stated above.

Specifically, unlike the second mode of vibration, in the third mode, there was necessary strain energy in the joint, as shown in Fig. 16c. The mode shape was also sufficient at the excitation point for the third mode to be excited to a relatively high level, as shown in Figs. 14c and 15c. These conditions enabled the third mode of vibration to be excited effectively which provided the source of detectable frictional heat generation in the joint as shown in Fig. 22, even though it was not directly targeted by the excitation force.

6 Discussions and conclusions

In this research, a modal-based vibrothermographic approach was studied and applied to evaluate the integrity condition of bolted joints in coupled structures.

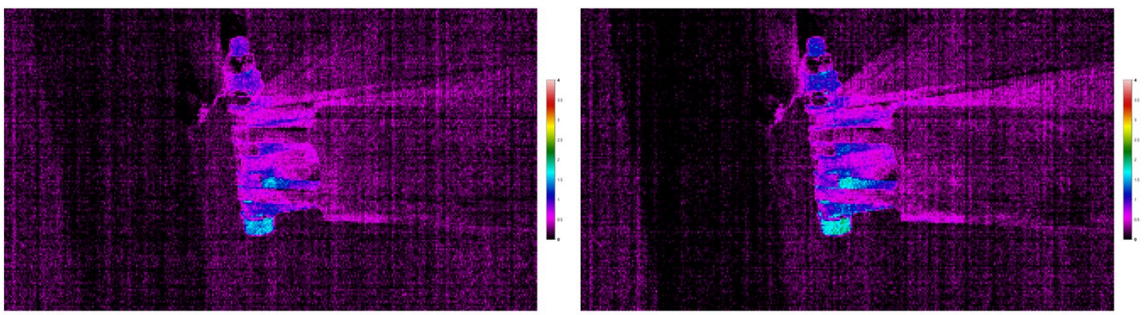

Fig. 22 The **a** first and **b** second snapshots from the final test using the second mode of vibration

Besides being successful in detecting the heat generated in loosening bolted joints during vibration, the proposed approach has been able to reveal the relationship between the frictional heat generation and the condition of vibrating bolted joints. Following the observations acquired during this research, the procedure for practical application of this modal-based vibrothermographic approach when utilized to evaluate integrity condition of bolted joints can be summarized.

Firstly, when data traceability is available, the frictional heat generation rate in the inspected joint should be used as the indication of failure. As described previously, the relationship between the frictional heat generation rate and the integrity condition of the bolted joint should be approximately described as a bell curve, unless the opening force exerted onto the joint during vibration is significant compared to the bolt load so that the loss of contact becomes dominant.

Based on this premise, given that other major parameters remain mostly unchanged, if the frictional heat generation rate stays approximately constant, the condition of the joint should be relatively stable. When the frictional heat generation rate increases, it can be an indication that the joint starts to fail. After continuous increases, when the frictional heat generation rate starts to decrease, it should be alarmed that the bolted joint is likely to approach failure.

Additionally, it has been demonstrated that the contact load in the bolted joints that corresponds to the maximum frictional heat generation rate is positively correlated with the force exerted onto the joint during vibration. This phenomenon can be useful in practical applications. Since joints experiencing greater forces during vibration are more likely to have more rapid failing processes, having earlier indications of the potential failure of the joints will undoubtedly improve the safety of the structure.

In circumstances where the significant loss of contact between surfaces is unavoidable so that the relationship between joint condition and frictional heat generation rate becomes monotonic, it is still possible to rely on frictional heat generation rate as the indication of damage. However, a properly determined threshold must be selected, and actions need to be taken once the frictional heat generation rate falls below this threshold.

When data traceability is unavailable, determining the stage of a joint in its failing process is considerably more difficult. Even for a well-calibrated structure for which the exact relationship between the frictional heat generation rate and the joint integrity condition is established, a point with acknowledged frictional heat generation rate may still be located at either side of the plot because of the bell-curve-shaped relationship. If a joint close to failure is falsely determined as a sound joint because of their similar values of frictional heat generation rate, catastrophic failures might happen. For this reason, online monitoring of joints in critical regions appears to be necessary in order to allow data traceability.

Besides, it was also demonstrated that the temperature increase representing the heat generation can be as an indication of the damping ratio of a structure, which could be particularly useful when direct measurement of damping data is difficult, such as when the inspected structure or region is physically inaccessible.

Apart from major conclusions summarized above, it has also been verified that this modal-based vibrothermographic method is still able to work even if the structure does not vibrate at a resonant frequency of a mode of vibration with high strain energy in the joint. The adjacent modes of vibration excited at their residual responses are possible to provide necessary strain energy in the joint, which aids the frictional heat generation. Apart from evaluating joint integrity, this phenomenon can also be used in the detection of other types of damage based on vibrothermography, where the non-targeted modes of vibration are also able to provide strain energy in the damaged region.

7 Potential and future work

Other than the activities completed during this research, this vibrothermographic approach also has potential in other relevant areas. For this reason, future work has been planned as possible extensions of this research.

Firstly, in the planning phase of the vibrothermographic tests, the distribution of the strain energy in the structure during vibration was calculated through FE analyses due to the limitations on the actual number of sensors that can be placed on the physical structure. However, a full-field strain measurement—rather than sparse strain gauge measurements—performed directly on the physical structure could be particularly useful for this application, should the experimental infrastructure be available.

Secondly, it is worthwhile to establish a method for detecting the loss of contact in relevant regions and evaluating its influence on the thermal parameters in vibrothermographic tests. This may be achieved by experimental methods or data processing techniques such as motion amplification. Motion amplification can magnify the subtle motion in engineering structures so that they become more apparent, with which the dynamic behaviors in the contact regions can be more easily observed and evaluated.

Thirdly, the proposed vibrothermographic approach, when utilized to evaluate the integrity condition of bolted joints, relies on traceability of data from which a trend

of frictional heat generation can be established. For the generality of this approach, the possibility of determining joint conditions without traceable data should be studied. It is possible that this can be achieved by observing other phenomena, such as the distribution of frictional heat generation across multiple interfaces, which has been briefly mentioned at the end of the experimental vibrothermographic testing section.

Additionally, in this research, the temperature of the hot spots observed in the experimental tests was generally 1 °C to 5 °C higher than the surrounding regions during the vibration caused by the single-point single-frequency excitation. In other applications, these values could be either higher or lower depending on the parameters of the excitation force(s) directly affecting the amplitude and the shape of the vibration. However, considering that modern IR cameras are usually able to achieve a sensitivity of lower than 0.05 °C in a regular room-temperature environment, the hot spots caused by the frictional heat generation should be able to capture these phenomena in most situations. Apart from the net temperature increases, the ambient temperature during the experimental tests in this research was relatively unchanged at regular room temperature (approximately 20 °C) so that the extra factors related to ambient temperature were not major concerns. However, many coupled engineering structures, such as aircraft engines, usually operate in a significant ambient temperature. Such high ambient temperature is likely to raise several problems not covered in this research. Firstly, high temperature will cause thermal expansion of materials, which may significantly affect the relationship between the frictional heat generation and the internal load within the joints because of the altered contact conditions. Secondly, the performance such as accuracy and sensitivity of IR cameras usually depend on the operating and the background temperature. A relatively small temperature increase caused by friction might become difficult to detect in a high-temperature environment. For this reason, additional tests might be performed to study the effectiveness of this vibrothermographic approach in these conditions.

Similarly, the upper limit of the bolt load that was studied experimentally in this research was 6.0 Nm, which was approximately the maximum bolt load that could be applied by hand on the bolt in the frame structure. For different structures, this value usually varies from case to case, depending on the physical parameters of the joint to be studied. Additional research on a wider range of bolted structures with different bolt load levels would be appropriate for alternate applications.

Lastly, as demonstrated in this article, thermal parameters such as the temperature increases can be used to reveal changes in dynamic properties like the damping ratio. It may be possible to rely on vibrothermography as an indirect measurement approach of other dynamic properties in relevant applications where direct measurement methods cannot be easily applied.

Acknowledgements The finite element analyses of this work were carried out using the computational facilities of the Advanced Computing Research Centre, University of Bristol—https://www.bris.ac.uk/acrc/.

Availability of data and material The data produced during this research project and used in this article have been uploaded to Google Drive. The files can be accessed at https://drive.google.com/drive/folders/1C_WzgNTSp0bzB6JkC43piuIgXV4Nqt1v?usp=sharing. Due to the significant size of the output files from the time-domain finite element analyses, only the corresponding input files have been uploaded. The input files require SIMULIA Abaqus in order to process.

Compliance with ethical standards

Conflict of interest The authors declare that they have no conflict of interest.

References

1. Ibrahim RA, Pettit CL (2005) Uncertainties and dynamic problems of bolted joints and other fasteners. J Sound Vib 279(3–5):857–936
2. Gaul L, Lenz J (1997) Nonlinear dynamics of structures assembled by bolted joints. Acta Mech 125(1–4):169–181
3. Schwingshackl CW, Di Maio D, Sever IA, Green JS (2013) Modeling and validation of the nonlinear dynamic behavior of bolted flange joints. J Eng Gas Turb Power 135(12)
4. Hartwigsen CJ, Song Y, McFarland DM, Bergman LA, Vakakis AF (2004) Experimental study of non-linear effects in a typical shear lap joint configuration. J Sound Vib 277(1–2):327–351
5. Ma X, Bergman L, Vakakis A (2001) Identification of bolted joints through laser vibrometry. J Sound Vib 246(3):441–460
6. Di Maio D (2016) Identification of dynamic nonlinearities of bolted structures using strain analysis. In: Experimental validation of pseudo receptance difference (PRD) method for nonlinear model updating, Springer, pp 387–414
7. Di Maio D, Bozzo A, Peyret N (2016) Response phase mapping of nonlinear joint dynamics using continuous scanning LDV measurement method. In: Proceedings of the 12th international a.i.ve.la. conference on vibration measurements by laser and noncontact techniques: advances and applications, Ancona

8. Chi X, Di Maio D, Lieven NAJ (2018) Dynamic response and energy loss in jointed structures using finite element methods: application to an aero-engine casing assembly. In: Proceedings of international conference on noise and vibration engineering, ISMA2018, Leuven
9. Clayton EH, Kennel MB, Fasel TR, Todd MD, Stabb MC, Arritt BJ (2008) Active ultrasonic joint integrity adjudication for real-time structural health monitoring. In: Proceedings of SPIE—the international society for optical engineering, May 2008
10. Fierro GPM, Meo M (2018) IWSHM 2017: structural health monitoring of the loosening in a multi-bolt structure using linear and modulated nonlinear ultrasound acoustic moments approach. Struct Health Monit 17(6):1349–1364
11. Doyle DT, Zagrai A, Arritt B (2009) Bolted joint integrity for structural health monitoring of responsive space satellites. In: 50th AIAA/ASME/ASCE/AHS/ASC structures, structural dynamics, and materials conference, Palm Springs, California, 4–7 May 2009
12. Argatov I, Sevostianov I (2010) Health monitoring of bolted joints via electrical conductivity measurements. Int J Eng Sci 48(10):874–887
13. Shin HJ, Yun CY, Park G, Farinholt KM, Lee JR, Park CY, Jun SM, Farrar CR (2012) Assessing joint integrity of a lug assembly using piezoelectric active sensors. Struct Control Health Monit 19(7):621–631
14. Zagrai A, Doyle D, Gigineishvili V, Brown J, Gardenier H, Arritt B (2010) Piezoelectric wafer active sensor structural health monitoring of space structures. J Intell Mater Syst Struct 21(9):921–940
15. Giurgiutiu V, Reynolds A, Rogers CA (1999) Experimental investigation of E/M impedance health monitoring for spot-welded structural joints. J Intel Mater Syst Struct 10(10):802–812
16. Pavelko I, Pavelko V, Kuznetsov S, Ozolinsh I (2014) Bolt-joint structural health monitoring by the method of electromechanical impedance. Aircr Eng Aerosp Technol 86(3):207–214
17. Kim J, Wang K-W (2018) Electromechanical impedance-based damage identification enhancement using bistable and adaptive piezoelectric circuitry. Struct Health Monit 18(4):1268–1281
18. Meola C, Boccardi S, Carlomagno GM (2016) Infrared thermography in the evaluation of aerospace composite materials: infrared thermography to composites. Woodhead Publishing, Cambridge
19. Chi X, Di Maio D, Lieven NAJ (2019) Modal-based vibrothermography using feature extraction with application to composite materials. Struct Health Monit. https://doi.org/10.1177/1475921719872415
20. Stepinski T, Uhl T, Staszewski W (2013) Advanced structural damage detection: from theory to engineering applications. Wiley, New York
21. Henneke EG II, Reifsnider KL, Stinchcomb WW (1986) Vibrothermography: investigation, development, and application of a new nondestructive evaluation technique. Virginia Polytechnic Institute and State University, Blacksburg
22. Ewins DJ (1984) Modal testing: theory and practice. Wiley-Blackwell, Hoboken
23. Dieterich JH (1978) Time-dependent friction and the mechanics of stick-slip. Pure Appl Geophys 116(4–5):790–806
24. Woodhouse J, Putelat T, McKay A (2015) Are there reliable constitutive laws for dynamic friction? Philos Trans R Soc A Math Phys Eng Sci 373(2051):20140401
25. Leine RI, van Campen DH, de Kraker A, van den Steen L (1998) Stick-slip vibrations induced by alternate friction models. Nonlinear Dyn 16(1):41–54
26. Popp K, Stelter P (1990) Stick-slip vibrations and chaos. Philos Trans Phys Sci Eng 332(1624):89–105
27. Renshaw JB, Chen JC, Holland SD, Thompson RB (2011) The sources of heat generation in vibrothermography. NDT E Int 44(8):736–739
28. Dassault Systèmes (2018) Thermal contact properties. In: SIMULIA User Assistance 2018
29. Unbrako (2009) High-temperature joints. In: Multidisciplinary design project databook, The Cambridge-MIT Institute, pp 232–234
30. Dassault Systèmes (2018) Three-dimensional solid element library. In: SIMULIA User Assistance 2018
31. Sullivan JF (1988) Technical physics. Wiley, New York
32. Dassault Systèmes (2018) Contact constraint enforcement methods in Abaqus/Explicit. In: SIMULIA User Assistance 2018
33. Dassault Systèmes, "Natural frequency extraction," in *SIMULIA User Assistance 2018*, 2018.
34. Dassault Systèmes (2018) Predefined fields. In: SIMULIA User Assistance 2018
35. du Bois JL (2009) Adaptive fuselage response suppression. University of Bristol, Bristol